An analysis of spatiotemporal variations of soil and vegetation moisture from a 29-year satellite-derived data set over mainland Australia

Yi Y. Liu,[1,2] Albert I. J. M. van Dijk,[2] Richard A. M. de Jeu,[3] and Thomas R. H. Holmes[3]

[1] The spatiotemporal behavior of soil and vegetation moisture over mainland Australia was analyzed using passive microwave observations by four satellites going back to late 1978. Differences in measurement specifications prevented merging the data directly. A continuous product was developed for Australia by scaling percentiles of the cumulative moisture distribution within each grid cell to the percentiles of a reference sensor. The coefficient of correlation and root-mean-square error between rescaled values and the reference generally suggest good agreement. Using the merged data product, a strong El Niño–Southern Oscillation signal in near-surface hydrology across Australia was confirmed. Spatial patterns of trends in annual averages show that western and northwestern Australia have experienced an increase in vegetation moisture content, while the east and southeast experienced a decrease. Soil moisture showed a similar spatial pattern but with larger regions experiencing a decrease. This could be explained by decreasing rainfall and increasing potential evapotranspiration during the extended winter period (May–September). The results give us reasonable confidence in the time series of soil and vegetation moisture derived by the scaling method developed in this study. Development of a global data set along these lines should enable better estimation of hydrological variables and should increase understanding of the impacts of ocean circulations on terrestrial hydrology and vegetation dynamics.

Citation: Liu, Y. Y., A. I. J. M. van Dijk, R. A. M. de Jeu, and T. R. H. Holmes (2009), An analysis of spatiotemporal variations of soil and vegetation moisture from a 29-year satellite-derived data set over mainland Australia, *Water Resour. Res.*, *45*, W07405, doi:10.1029/2008WR007187.

1. Introduction

[2] Soil moisture plays an important role in water and energy balance at the interface between the land surface and the atmosphere, and this role has been studied with various models regionally and globally [*Cherkauer et al.*, 2003; *Dickinson et al.*, 1986; *Liang et al.*, 1994; *Wigmosta et al.*, 1994; *Wood*, 1991]. Previous studies indicate that the assimilation of passive microwave observed near-surface soil moisture can reduce errors in forecasting soil moisture profile as a result of poor initialization and improve the resulting predictions of runoff and evapotranspiration [*Pauwels et al.*, 2001; *Walker and Houser*, 2001; *Wigneron et al.*, 1999]. *Reichle et al.* [2007] found that the estimates from the assimilation of soil moisture retrievals from passive microwave observations are superior to those from the satellite or model data alone. That is, long-term passive microwave observations of near-surface soil moisture can be utilized for more accurate and reliable estimates of deeper soil moisture, evapotranspiration and runoff, and consequently better understanding of feedback mechanisms between different hydrological components, but such a long-term soil moisture data set is not currently available.

[3] A recently developed approach to retrieving surface parameters from microwave emissions can in principle be used for all low-frequency bands (<20 GHz) in the microwave domain [*De Jeu and Owe*, 2003; *Owe et al.*, 2001, 2008; *Wagner et al.*, 2007]. This approach enables us to collect the worldwide data of soil moisture and vegetation water content by four different satellites since late 1978. However, these four satellites cover different time periods and differences in measurement specifications of different instruments prevent merging the data directly.

[4] The objective of this paper is twofold. First is to develop a methodology to merge a 29-year time series of soil moisture and vegetation optical depth compiled from different passive microwave instruments covering the period from October 1978 through December 2006 across mainland Australia.

[5] The second aim is to evaluate the merged product through statistical analyses. Using the moisture retrievals from the TRMM satellite (1998–2005) only, *Liu et al.* [2007] investigated the spatiotemporal patterns in soil and vegetation moisture across Australia. The results suggested that the drought conditions in eastern Australia since 2000 have a strong connection with El Niño. During El Niño

[1]School of Civil and Environmental Engineering, University of New South Wales, Sydney, New South Wales, Australia.
[2]Black Mountain Laboratory, CSIRO Land and Water, Canberra, ACT, Australia.
[3]Department of Hydrology and Geo-Environmental Sciences, Faculty of Earth and Life Sciences, Vrije Universiteit, Amsterdam, Netherlands.

Table 1. Comparisons of Major Characteristics of Six PM Instruments on Four Satellites

	SMMR	SSM/I	TMI	AMSR-1
Platform	Nimbus 7	DMSP F8, F11, F13	TRMM	AQUA
Time series	Oct 1978 to Aug 1987	F8, Sep 1987 to Dec 1991; F11, Dec 1991 to Sep 1995 F13, May 1995 to present	Dec 1997 to present (boosted in Aug 2001)	May 2002 to present
Channel used (GHz)	6.6	19.3	10.7	6.9
Spatial resolution (km)	150	69 × 43	59 × 36	76 × 44
Spatial coverage	global	global	N38° to S38°	global
Swath width (km)	780	1400	780, after boost 897 km	1445
Approximate equatorial crossing time	ascending, noon; descending, midnight	F8, ascending, 0630; F11/13, descending, 0630	completing an orbit every 91 min, making 15.7 orbits per day	ascending, 1330; descending, 0130
Temporal resolution	alternate day	daily	several times per day	several times per day

events, droughts are normally experienced in Australia and consequently a reduction in vegetation and primary production occurs [*Ogallo*, 1988; *Ropelewski and Halpert*, 1987]. However, the period from 1998 through 2005 only covered the moderate 2002 El Niño event. Using a merged data set covering from late 1978 through 2006, we will reinvestigate the impacts of the El Niño–Southern Oscillation (ENSO) on soil moisture and vegetation condition across mainland Australia to identify whether the high correlations found in the previous study are maintained. In addition, we perform a linear trend analysis to detect the long-term change in soil and vegetation moisture over the study period. As a means of evaluation of the merged product, we will compare these with the results of similar correlation and trend analysis using interpolated rainfall observations and soil moisture derived from macroscale hydrology models for the same period.

2. Data and Methods

2.1. Soil Moisture and Optical Depth

[6] The passive microwave (PM) data used in this study are derived from six separate instruments on four missions: the scanning multichannel microwave radiometer (SMMR) on board the Nimbus 7 satellite, the Special Sensor Microwave Imager (SSM/I) on the F8, F11 and F13 satellites from the Defense Meteorological Satellite Program (DMSP), the microwave imager from the Tropical Rainfall Measuring Mission (TRMM), and the Advanced Microwave Scanning

Radiometer–Earth Observing System (AMSR-E) aboard the Aqua satellite. All sensors have several common wave bands, while some additional wave bands are either unique or common to only two or three of the satellite systems. Specifications for the different sensors are listed in Table 1. The best estimates of soil and vegetation moisture can be expected from the radiometers with the lowest frequency (i.e., SMMR with 6.6 GHz and AMSR with 6.9 GHz), but the available observations mean that sometimes less optimal frequencies need to be used.

[7] Both soil moisture (θ, m^3 m^{-3}) and vegetation optical depth (τ, dimensionless) were retrieved from brightness temperatures (T$_B$) observed by different satellites using the Land Parameter Retrieval Model (LPRM) [*Owe et al.*, 2008]. Optical depth (τ) can be interpreted as an indicator of the canopy density that is directly proportional to vegetation water content at any certain frequency [*Jackson and O'Neill*, 1990; *Jackson and Schmugge*, 1991] and was derived following *Meesters et al.* [2005].

[8] Figure 1 shows time periods of θ and τ retrievals from different instruments used in this study. SSM/I retrievals are only available for the F8, F11 and F13, which is limited by the availability of SSM/I T$_B$ data products from the National Snow and Ice Data Center (NSIDC).

2.2. Data Quality Control

[9] Microwave frequency and overpass time are two important factors that influence the absolute value of retrieved θ and τ [*Cashion et al.*, 2005; *Derksen et al.*,
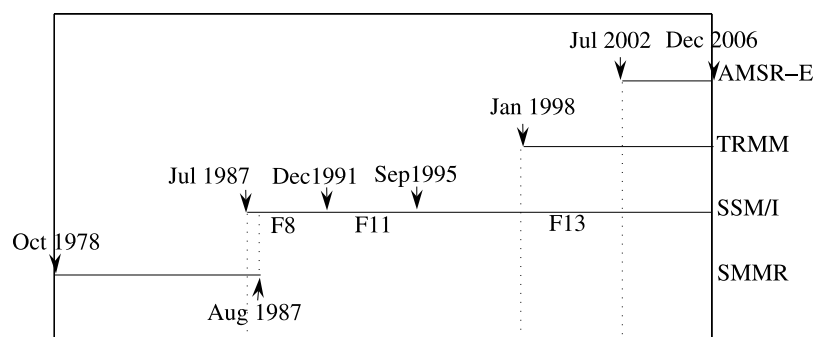
Figure 1. Time span of available soil and vegetation moisture estimates retrieved from different satellites used in   udy.

Figure 2. Map of Australia (10°S–40°S, 110°E–160°E) showing the extent of missing SSM/I θ retrievals for tropical northern Australia throughout the whole year. Most likely, data missing is due to the dense vegetation cover and high microwave frequency of SSM/I.

2000]. In theory, lower microwave frequency leads to more accurate estimates; with increasing microwave frequency, the attenuation by vegetation increases [*Jackson and Schmugge*, 1995; *Njoku and Entekhabi*, 1996]. Hence θ and τ retrievals used in this analysis were derived from the lowest microwave frequency of each instrument. Diurnal variation of soil temperature and moisture content may be considerable [*Raju et al.*, 1995] and therefore the time of overpass can influence absolute retrieved θ. We used the observations acquired by ascending passes of SSM/I F8 and descending passes of SSM/I F11/13, which have similar overpass time, around 6:30 A.M. local time. For SMMR and AMSR-E, only the observations acquired by descending passes were used as the minimal temperature gradients at midnight are more favorable for the retrievals [*De Jeu*, 2003].

[10] The retrieved θ and τ were resampled from the original resolution (Table 1) into daily averages at 0.25° (about 25 km) for late 1978 through 2006 for mainland

Australia. (Tasmania was excluded because it is not covered by the TRMM satellite.) Spatial resampling was conducted before the temporal resampling. If a grid cell had more than one value per day, then all values for that day were averaged. The resampled daily data was further converted to monthly averages. Because of power constraints on the platform and the considerably narrower swath width for SMMR, there are only up to around five soil moisture retrievals from descending passes per month for SMMR. A monthly average calculated from more than three daily values was considered valid.

[11] As stated, the attenuation by vegetation increases with increasing microwave frequency, which may result in invalid θ retrievals over the regions with highly dense vegetation. In this analysis, some SSM/I θ retrievals are missing for the tropical northern Australia throughout the whole year (Figure 2). Over the southeast coastal region and the southwest of Western Australia, some SSM/I θ retrievals are missing for two or three months every year. The most likely reason is that the Ku band wavelength of SSM/I is too short to penetrate the dense vegetation cover. Missing data is rarely observed in θ retrievals from SMMR, TRMM or AMSR-E.

[12] The drift of the SSM/I sensor could be an issue, particularly when deriving long-term trends [*Wentz and Schabel*, 2000]. The information from the National Snow and Ice Data Center [*Armstrong et al.*, 1994] and the Remote Sensing Systems (RSS) indicate that the ascending equatorial time of F8 at launch was 6:15 A.M. and almost no sensor drift was detected until it was decommissioned in December 1991. The descending equatorial time of F11 drifted from 6:11 A.M. to 6:25 A.M. between December 1991 and September 1995, while F13 has drifted from 5:42 A.M. to 6:33 A.M. since launched in 1995.

[13] We examined monthly averages of SSM/I θ retrievals over the period from 1987 through 2006. The fluctuations are in agreement with the rainfall variations for the same period, e.g., relatively wet in 1989, 1999, 2000 and 2001, and relatively dry during 1992 through 1995 and 2002/2003. No significant drift of absolute values of retrieved θ was observed. Hence, the impact of SSM/I sensor drift on this study is considered acceptable. The most likely reason
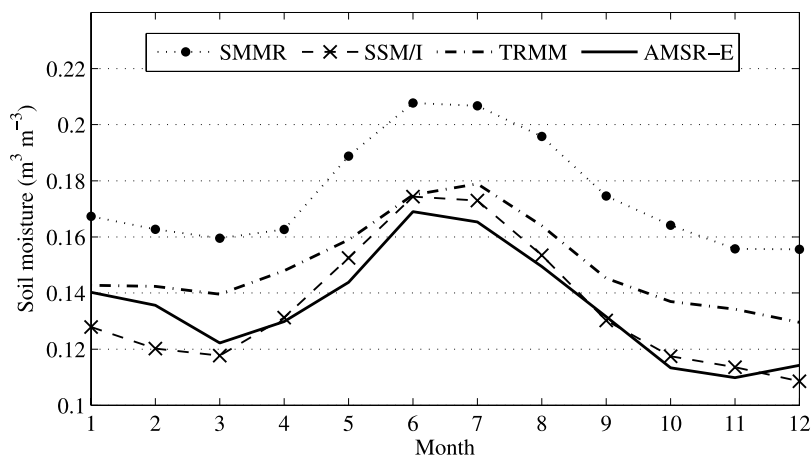

Figure 3. Monthly average of θ retrievals from SMMR, SSM/I, TRMM, and AMSR-E over mainland Australia exclu   e tropical north with missing data shown in Figure 2.
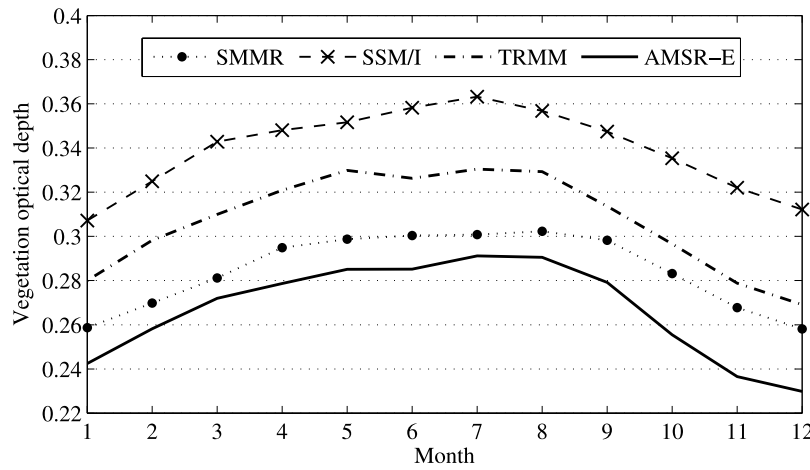
Figure 4. Continental monthly average of τ retrievals from SMMR, SSM/I, TRMM, and AMSR-E.

is that there is little change in moisture dynamics during the overpass time—approximately between 5:30 A.M. and 6:30 A.M. No significant drift was observed in the monthly SSM/I τ retrievals.

2.3. Data Merging

[14] Differences in sensor specifications, particularly different microwave frequencies and spatial resolutions, result in different absolute values of estimated θ and τ. Figure 3 shows monthly averages of θ retrievals from different instruments over mainland Australia excluding the tropical north with missing data shown in Figure 2. Figure 4 shows the continental monthly averages of τ retrievals. For θ, the satellite observations represent a soil sampling depth ranging from about 0.5 cm to 1.5 cm, depending on the microwave frequencies [Owe et al., 2008]. Kirdiashev et

al. [1979] stated that τ is directly related to the wavelength and therefore it differs at different frequencies. Additionally, varying absolute values can be partially attributed to different original spatial resolutions. For example, SMMR has a coarse spatial resolution ($\sim$150 km); thus the influence of ocean water on the microwave signals extends further inland and may leads to relatively high absolute values of SMMR retrievals.

[15] Despite θ and τ retrieved from different instruments having different absolute values, they show similar seasonal patterns, which creates the possibility for rescaling and merging to yield a long-term data set. AMSR-E was selected as the reference against which other θ and τ retrievals are rescaled, because it has a relatively low measuring frequency, high spatial and temporal resolution, and is still operational.
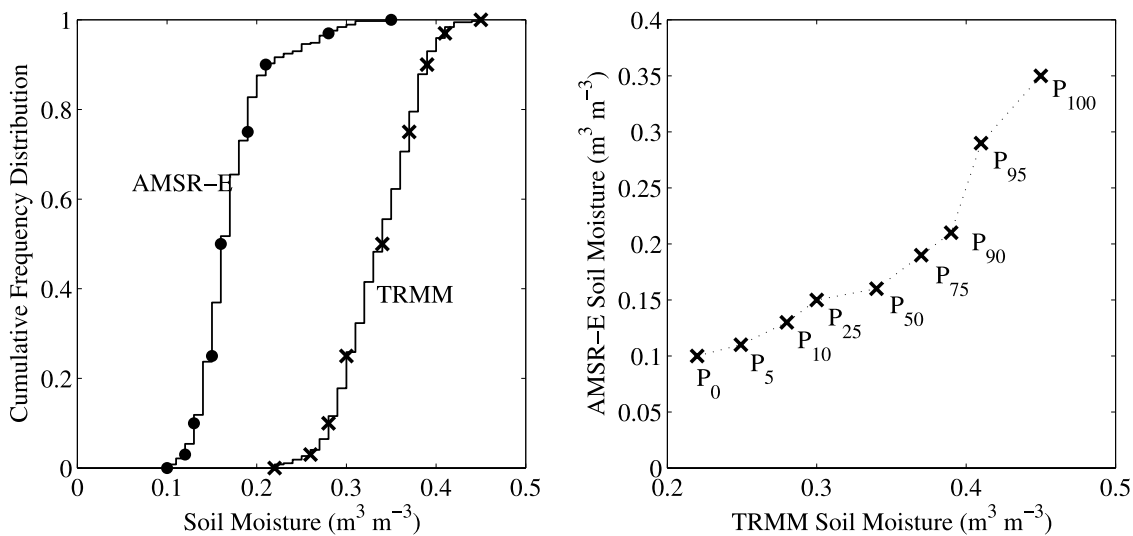

Figure 5. (left) Cumulative frequency distributions of θ of an example grid cell at 24.5°S, 114°E. TRMM retrievals were adjusted against AMSR-E retrievals. The 0th, 5th, 10th, 25th, 50th, 75th, 90th, 95th and 100th percentiles of AMSR-E and TRMM are marked, dividing the distribution of θ into eight segments. (right) Regression lines of TRMM against AMSR-E. Data in different segments have different adjusting equatio
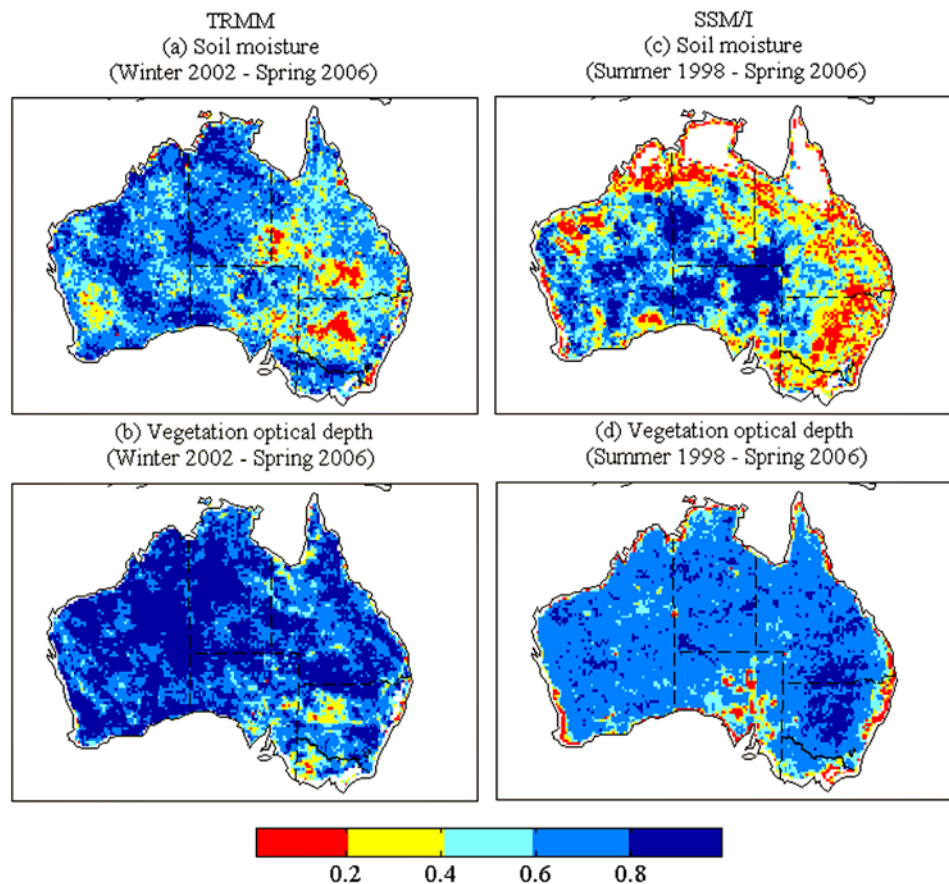
Figure 6. (a and b) R^2 between TRMM* and AMSR-E (after removing the seasonal cycle) for the overlapping period (winter 2002 to spring 2006). (c and d) R^2 between SSM/I* and TRMM*−AMSR-E (after removing the seasonal cycle) for the overlapping period (summer 1998 to spring 2006).

[16] The cumulative distribution function (CDF) matching technique was chosen as the rescaling method. Similar CDF matching approaches have been successfully used in the past. *Reichle and Koster* [2004] merged satellite soil moisture observations with model data by CDF matching, and both *Anagnostou et al.* [1999] and *Atlas et al.* [1990] established reflectivity-rainfall relationships for calibration of radar or satellite observations of precipitation using CDF matching.

[17] The CDF method was applied cell by cell. One example is shown in Figure 5. The 0th, 5th, 10th, 25th, 50th, 75th, 90th, 95th and 100th percentiles of AMSR-E and TRMM were used to divide the cumulative distribution into eight segments. The same percentile values of TRMM are plotted against those of AMSR-E. Eight linear equations were obtained to adjust TRMM data falling into different segments against AMSR-E data.

[18] The rescaling procedure was applied on the monthly averages of θ and τ retrievals according to the following steps.

[19] 1. Rescale TRMM against AMSR-E using data for the overlapping period (July 2002 to December 2006) for the scaling parameters (linear equations).

[20] 2. Use the scaling equations derived from step 1 to rescale TRMM data for the period from January 1998 through June 2002, pro   rescaled TRMM (TRMM*,

hereafter * refers to rescaled values). When the data values to be rescaled in step 2 lie outside of the range of the data in step 1, we used the scaling equation of the closest value in the data in step 1.

[21] 3. Merge TRMM* (January 1998 to June 2002) with AMSR-E (July 2002 to December 2006), producing TRMM*−AMSR-E.

[22] 4. Rescale SSM/I against TRMM*−AMSR-E using data for the overlapping period (January 1998 to June 2004) for the scaling parameters.

[23] 5. Use the scaling equations derived from step 4 to rescale SSM/I data for the period from August 1998 through December 1997, producing SSM/I*. When the data values to be rescaled in step 5 lie outside of the range of the data in step 4, we used the scaling equation of the closest value in the data in step 4.

[24] 6. Merge SSM/I* (August 1987 to December 1997) with TRMM*−AMSR-E producing SSM/I*−TRMM*−AMSR-E.

[25] 7. Retrievals from SMMR capture the identical season pattern as SSM/I, TRMM and AMSR-E (Figures 6 and 7). The period of SSM/I*−TRMM*−AMSR-E (August 1987 to December 2006) covers the extremely wet year (2000) and dry year (2002); thus the range of SMMR retrievals should be within the range of SSM/I*− TRMM*−AMSR-E retrievals. We made the assumption
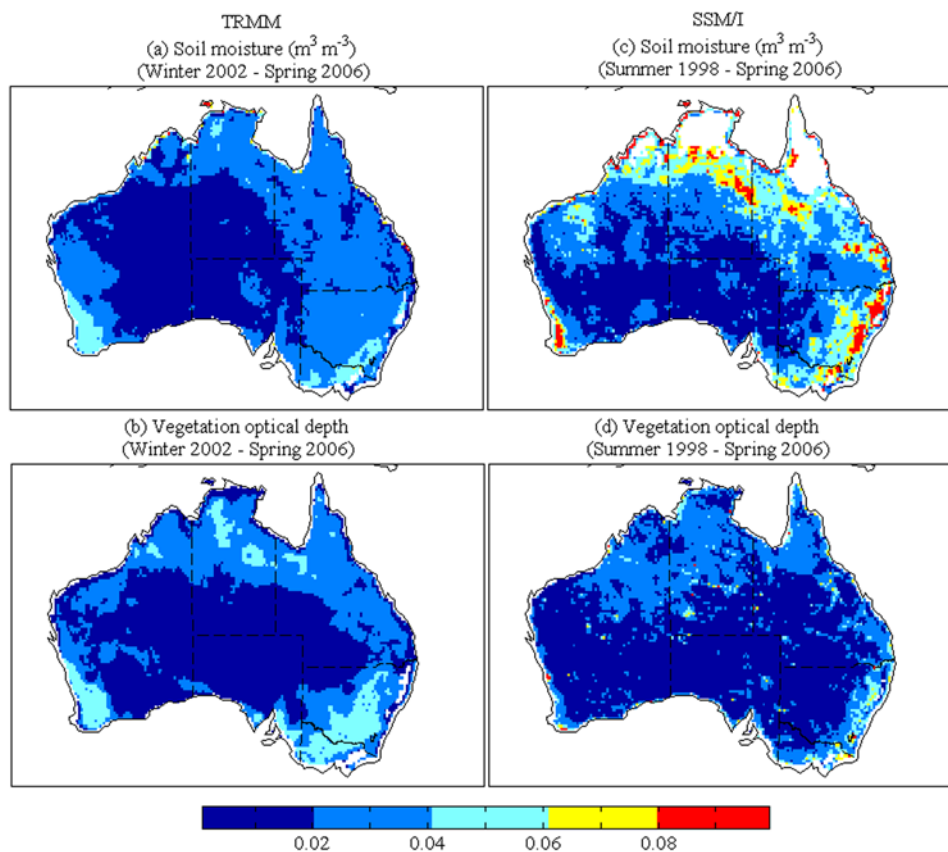
Figure 7. (a and b) RMSE between TRMM* and AMSR-E (after removing the seasonal cycle) for the overlapping period (winter 2002 to spring 2006). (c and d) RMSE between SSM/I* and TRMM*– AMSR-E (after removing the seasonal cycle) for the overlapping period (summer 1998 to spring 2006).

that the cumulative distribution of monthly values is identical for SSM/I*–TRMM*–AMSR-E as for SMMR, producing SMMR* (December 1978 to July 1987).

[26] 8. Obtain SMMR*– SSM/I*–TRMM*–AMSR-E (December 1978 to December 2006).

[27] The rescaled θ and τ were converted to seasonal averages for this study. Four seasons are defined as summer (December–February; summer 1979 refers to December 1978 to February 1979, and so on), autumn (March–May), winter (June–August) and spring (September–November). A season average calculated from at least 2 valid monthly data was considered valid. The analyses reported here refer to seasonal averages.

2.4. Southern Oscillation Index

[28] The ocean circulation indicator used in this study was the Southern Oscillation Index (SOI). The ENSO cycle of alternating warm El Niño and cold La Niña events is the dominant global climate signal, originating in the tropical Pacific through interactions between the ocean and the atmosphere [McPhaden et al., 2006]. The SOI used is the standardized anomaly of the mean sea level pressure difference between Tahiti and Darwin (Troup SOI) [McBride and Nicholls, 1983], and a time series was obtained from the Australia Bureau of Meteorology (http://www.bom.gov.au/ climate/current/soihtm1.shtml). During El Niño years, the SOI index is below average and below average rainfall is

often observed, while La Niña events during which the SOI index is above average often brings greater rainfall.

2.5. Statistical Methods

[29] Spearman's (nonparametric) correlation analysis was used in this study to investigate the correlations between seasonal θ, τ and rainfall versus the SOI. This was chosen because it does not require any assumptions about the nature of the relationship, as long as it is monotonic. Linear trend analysis was applied to detect the trend of the annual average and the spatial distribution of trends over the study period.

[30] The patterns in θ and τ would be expected to be related to rainfall, and to perhaps a lesser extent, potential evapotranspiration (PET). This provides an opportunity for a limited evaluation of merged data set. Gridded rainfall and PET data for mainland Australia for the same period were also included in the analysis for comparison. Gridded rainfall and PET data across Australia were interpolated from point observations by the Queensland Department of Natural Resources and Mines (http://www.longpad-dock.qld.gov.au/silo/). The original 0.05°-resolution gridded data was resampled into 0.25° resolution to allow direct comparison.

[31] In addition, soil moisture derived from macroscale hydrological models, the Community Land Model (CLM), Mosaic (MOS) and NOAH, generated by the Global Land
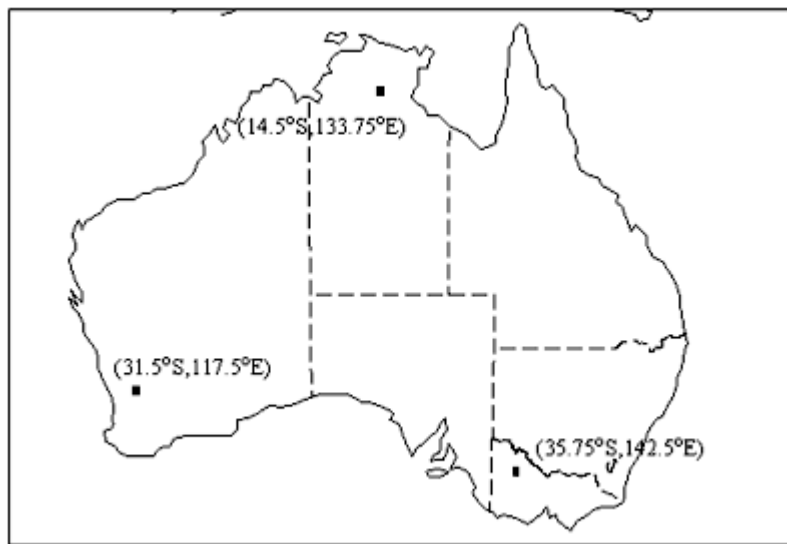
Figure 8. The locations of three selected grid cells: northern Australia (14.5°S, 133.75°E), southeastern Australia (35.75°S, 142.5°E), and southwestern Australia (31.5°S, 117.5°E).

Data Assimilation System (GLDAS) (ftp://agdisc.gsfc. nasa.gov/data/s4pa/GLDAS/) were included for comparison and evaluation purposes. The GLDAS was developed jointly by scientists from NASA and NOAA, aiming at generating optimal fields of water and energy cycle states and fluxes. It is a global offline terrestrial modeling system, ingesting satellite and ground-based observations by using advanced land surface modeling and data assimilation
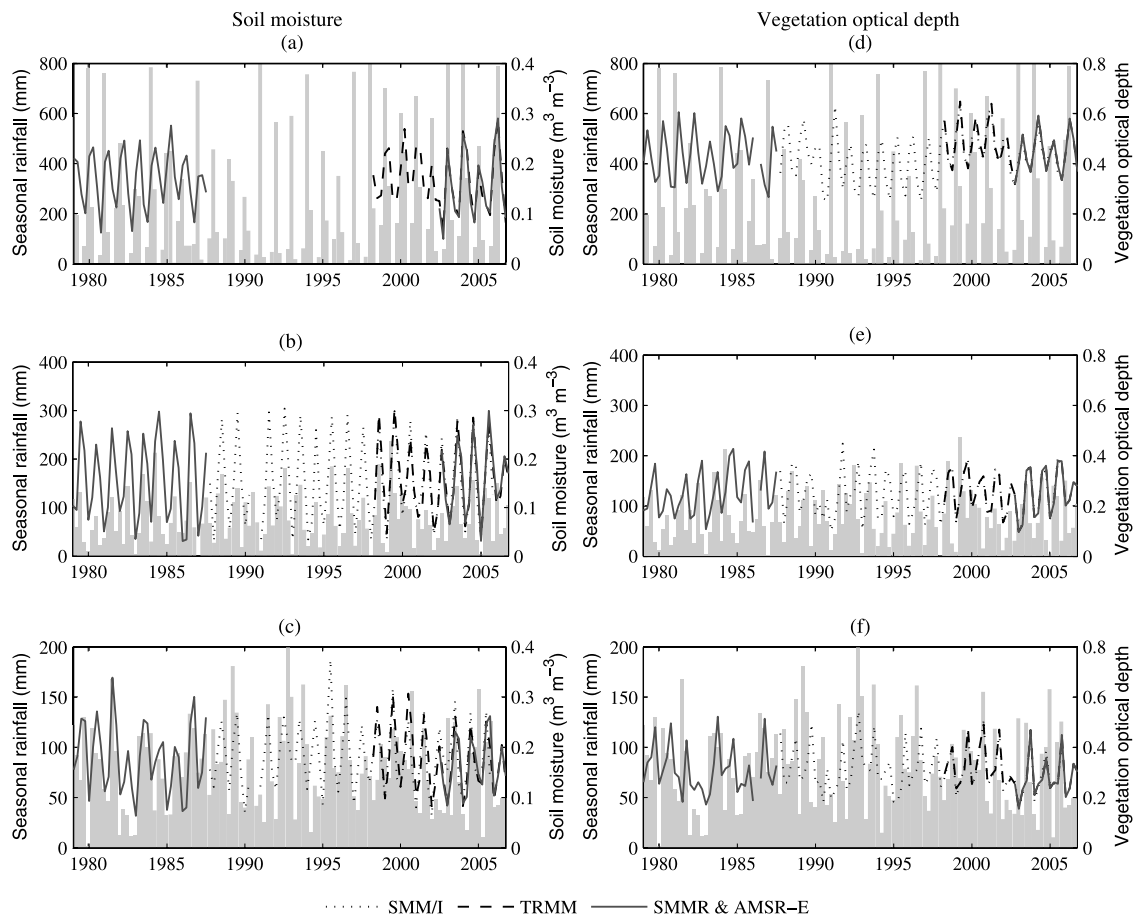

Figure 9. Seasonal average of rainfall, θ, and τ for three grid cells from (a and d) northern, (b and e) southeastern, a   nd f) southwestern Australia.
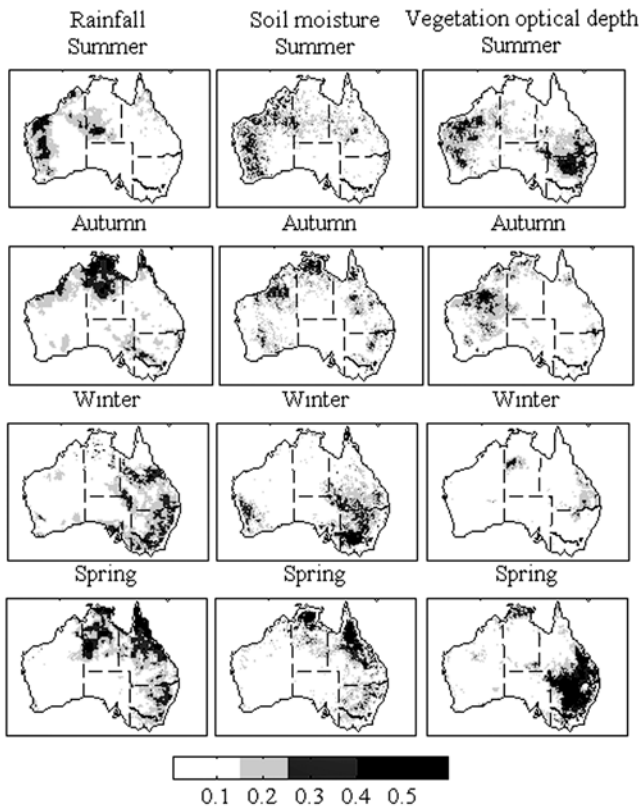
Figure 10. Spearman's correlation coefficients (r^2) between rainfall, θ, τ, and SOI index. Light gray regions are significant at $p = 0.05$ or better, and dark gray and black regions are significant at $p = 0.01$.

techniques [*Rodell et al.*, 2004]. The depths of the topsoil layer of these three models are 1.8, 2 and 10 cm, respectively, and the spatial resolution of these soil moisture products is 1°.

3. Results

3.1. Merging Data Sets

[32] Hereafter, θ and τ values refer to seasonal averages of merged SMMR*–SSM/I*–TRMM*–AMSR-E (summer 1979 to spring 2006) time series. To evaluate the uncertainty of the rescaled products, we removed the seasonal cycle and calculated the correlation coefficient (R^2) and root-mean-square error (RMSE) between residual rescaled θ and τ values and the reference (Figures 6 and 7). "Error" is not how differences should be interpreted, as both observations have heterogeneous uncertainties.

[33] Higher R^2 and lower RMSE suggest that the agreement between rescaled values and the reference is better. Figures 6 and 7 show that rescaled TRMM values (both θ and τ) agree well with the reference and so do the rescaled SSM/I τ retrievals. For the rescaled SSM/I θ retrievals, low R^2 and high RMSE are observed along the coast, particularly the eastern coast. This may be attributed to the relatively high microwave frequency of SSM/I (19.4 GHz) and dense vegetation in these coastal regions; with increasing frequency, the attenuation by vegetation increases and the accuracy of the estimat   eclines. The R^2 and RMSE

between SMMR* and SSM/I*–TRMM*–AMSR-E could not be calculated as they only have a very brief overlapping period (2 months).

[34] Seasonal rainfall, θ and τ for three locations (Figure 8) are shown in Figure 9. For the northern location, θ generally peaks in summer, which is in agreement with rainfall. τ peaks in autumn, one season behind θ. θ is missing from late 1987 through the end of 1997. This period is covered by SSM/I which has high microwave frequency of 19.4 GHz. It is observed that θ is rarely missing for the southeastern and southwestern locations during the same period, because the vegetation at these two locations is not as dense as in northern Australia. For the two southern locations, θ peaks simultaneously with rainfall in winter, and τ peaks in spring, which also reveals the lag between θ and τ.

3.2. Correlations With SOI

[35] The correlation of θ and τ retrievals with SOI was investigated using Spearman's correlation analysis. Figure 10 shows that the signals of SOI in θ retrievals are similar to rainfall and signals in τ are more or less one season behind rainfall and θ. Spring and winter are the most affected seasons. In winter, rainfall and θ over the east are influenced. In spring, SOI affects rainfall and θ over northern and eastern Australia, and τ in the southeast. SOI can explain more than 50% of the temporal variation of τ over the southeast in spring and θ over the north in winter. The winter/spring period is the wet season for southeastern and the dry season for northern Australia. In the dry season, zero rainfall and extremely low θ and τ are quite common in some northern and central parts; thus it is
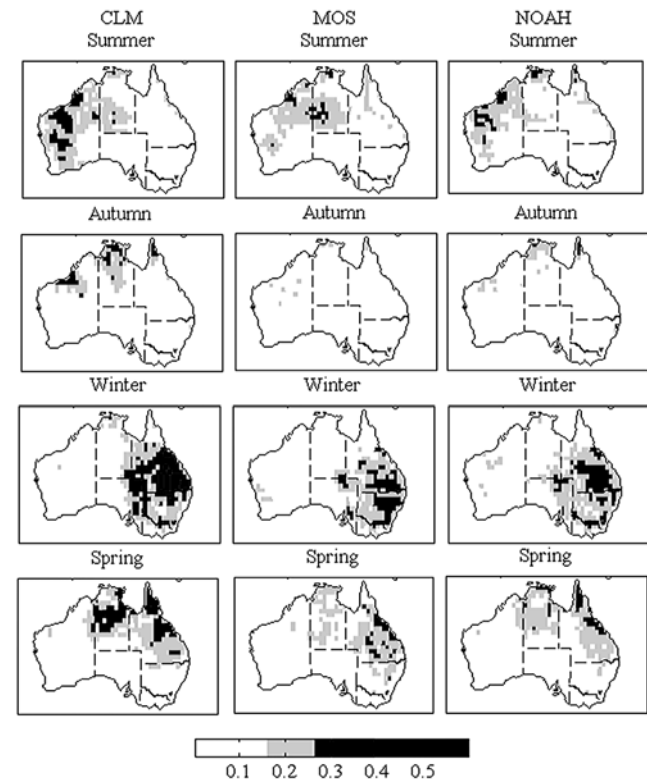

Figure 11. Same as Figure 10 but for model-derived θ from the CLM, MOS, and NOAH models. They represent θ from the top 1.8, 2, and 10 cm, respectively.
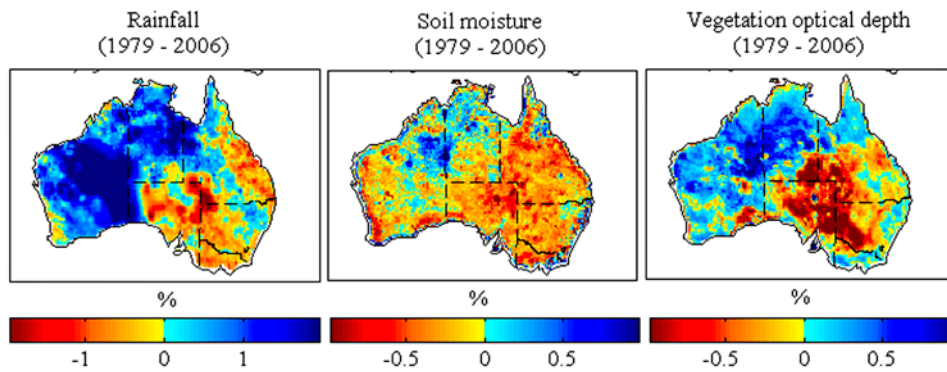
Figure 12. Spatial distributions of changes in annual rainfall, θ, and τ over the period from 1979 through 2006. The percentage represents the annual change relative to the average over the period from 1979 through 2006.

not surprisingly that the SOI has no significant effects in these regions.

[36] The correlation between model-derived θ and SOI was also presented for comparison and evaluation purposes (Figure 11). The spatial patterns of the correlations are comparable between remotely sensed and model-derived θ.

3.3. Trend Analysis

[37] Spatial patterns of simple linear trends in annual averages are shown in Figure 12. It is noted that these trends can in principle simply be the result of temporal rainfall distribution rather than reflecting a real underlying climate trend. In general, western and northwestern Australia experienced an increasing rainfall trend over the period from 1979 through 2006, while eastern and southeastern Australia experienced a decreasing trend. The regions with decreasing θ are larger than decreasing rainfall, particularly in the southwest of Australia. The spatial pattern of trend in τ is similar to rainfall. The results derived from modeled soil moisture also indicate that both eastern and southwestern Australia experienced decreasing trends during the analyzed period (Figure 13).

[38] The discrepancy of trends in annual rainfall and θ over the southwest of Australia can be explained by considering the seasonal pattern of rainfall and PET. For the southwest of Australia, extended winter (May–September) is the wetter season with great rainfall, low temperature and low PET; extended summer (October–

April) is the drier season with low rainfall, high temperature and high PET. Thus the annual θ is dominated by the rainfall and PET during the wetter season. Figure 14 shows that the wetter season became drier as a result of decreasing rainfall and increasing PET, and the drier season became wetter. The increasing rainfall in the drier season compensated the decreasing rainfall in the wetter season, resulting in the increasing annual rainfall. However, the annual θ still decreased because it is dominated by the changes in the wetter season. As for eastern Australia, the consistently decreasing rainfall and increasing PET lead to the decreasing θ and τ.

[39] As stated in section 2.2, θ derived from SMMR (1978–1987) were rescaled against θ retrieved from SSM/I, TRMM and AMSR-E (1987–2006) on the basis of the assumption that the range of SMMR retrievals should be within the range of SSM/I*–TRMM*–AMSR-E retrieval as they do not have any overlapping period. To comprehensively investigate the long-term changes in θ, the annual changes in rainfall, θ and τ over the period from 1988 through 2006 are calculated (Figure 15) and so are the θ derived from GLDAS models (Figure 16). As can be seen, satellite observed θ and τ, and model-derived θ show similar spatial patterns following the changes in rainfall for the same period. The western and northwestern Australia experienced an increasing rainfall trend over the period from 1988 through 2006, while eastern and southeastern Australia experienced a decreasing trend, which is in line
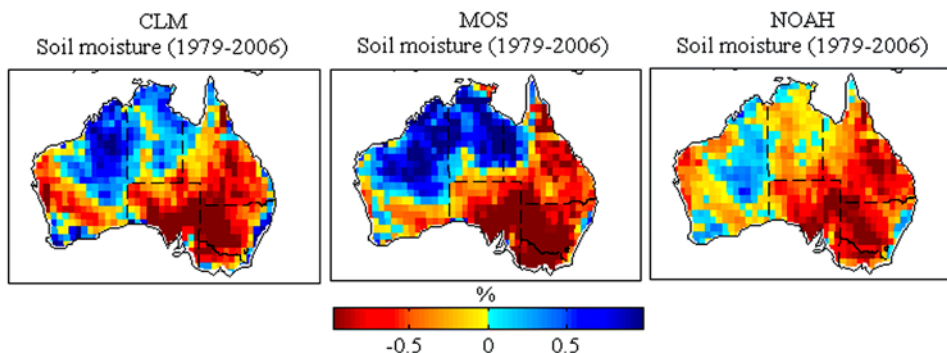

Figure 13. Same as Figure 12 but for model-derived soil moisture. The percentage represents the annual change relative to the average over the period from 1979 through 2006.
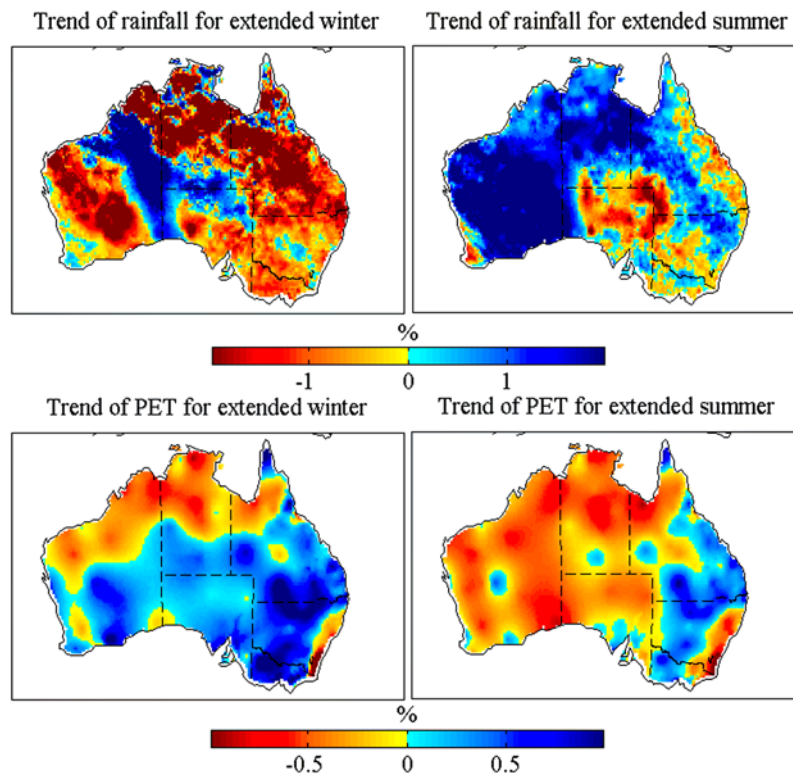
Figure 14. Spatial distributions of changes in the rainfall and potential evapotranspiration (PET) during extended winter (May–September) and summer (October–April) over the period from 1979 through 2006. The percentage represents the change per year relative to the average over the period from 1979 through 2006.

with the results of the longer term from 1979 through 2006 (Figures 13 and 14).

4.　Discussion and Conclusions

[40] The R^2 between seasonal TRMM* values and AMSR-E is generally greater than 0.6. The RMSE between seasonal θ from TRMM* and AMSR-E is mostly less than 0.04 m^3 m^{-3} and the RMSE of τ is less than 0.04. This illustrates that the TRMM* time series agrees well with AMSR-E. The R^2 and RMSE between seasonal τ from SSM/I* and TRMM*–AMSR-E are generally greater than 0.6 and less than 0.04, respectively. When removing the

seasonal signal, there is disagreement in θ anomalies ($R^2 <$ 0.2 and RMSE > 0.06) along the northern and eastern coast. The missing θ data over northern Australia are expected to be mainly due to the high microwave frequency of SSM/I (19.4 GHz) and dense vegetation in the north.

[41] The correlation analysis using 29 years of θ and τ retrievals and SOI index shows similar results to a previous study using the data of 8 years [Liu et al., 2007]. The dominant temporal and patterns are strongly correlated with SOI index in spring and winter, and to a lesser extent autumn and summer. This is also in line with the findings of Dai et al. [1997] that the SOI signal in precipitation is
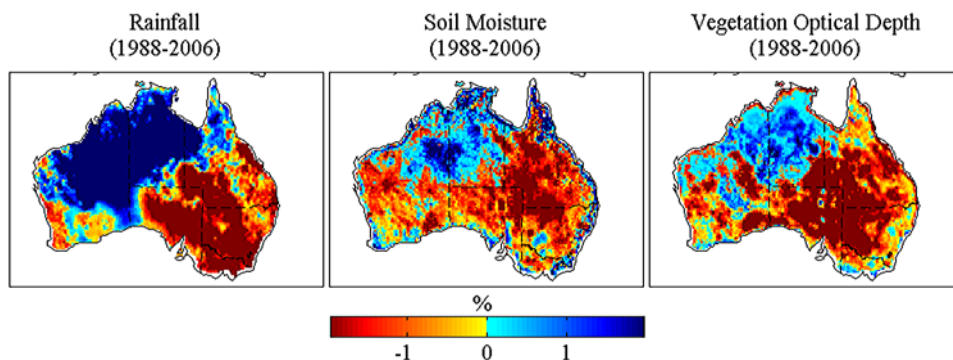

Figure 15. Spatial distributions of changes in annual rainfall, θ, and τ over the period from 1988 through 2006. The percentage represents the annual change relative to the average over the period from 1988 through 2006.
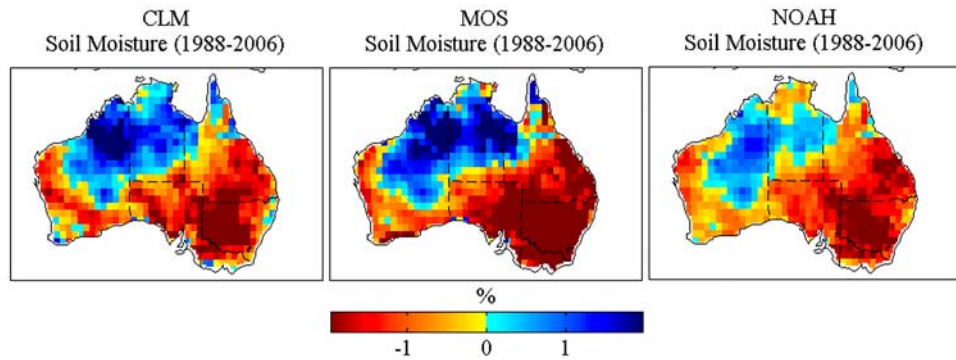
Figure 16. Same as Figure 15 but for model-derived soil moisture. The percentage represents the annual change relative to the average over the period from 1988 through 2006.

the strongest in spring (September–November) over the Australia-Indonesia region. The 29-year data covers several El Niño and La Niña events, and therefore our results provide further evidence that ENSO can be linked to the sequence of wet and dry conditions since late 1978.

[42] The consistently decreasing rainfall and increasing PET during the entire year over eastern and southeastern Australia result in declines in θ and τ. In southwestern Australia, the annual θ is dominated by the extended winter (May–September). With the decreasing rainfall and increasing PET during the extended winter, the trend in annual θ over southwestern Australia is negative.

[43] The merged product has uncertainties due to the inherent characteristics of passive microwave techniques and the CDF matching approach used in this study. At least in theory, lower microwave frequency leads to more accurate estimates; with increasing microwave frequency (shorter wavelength), the penetration ability of microwave declines and the attenuation by vegetation increases, even resulting in invalid θ retrievals (Figure 2). In this study, retrievals from TRMM (10.7 GHz) and SSM/I (19.3 GHz) are less accurate than those from SMMR (6.9 GHz) and AMSR-E (6.6 GHz), mainly because of more disturbing influences of vegetation. Varying microwave frequencies are associated with different soil sampling depths and vegetation optical depth signals. Therefore, both spatial and temporal errors of retrievals from different instruments are heterogeneous and may be propagated in the merged products in a complex manner. In addition, the CDF matching approach might affect the means of retrievals from SMMR, SSM/I and TRMM and the resulting trend of the merged products over the analyzed period. The uncertainty is greater in the SMMR* products, as SMMR has no overlapped period with other instruments and the rescaling is based on the assumption that the range of SMMR retrievals should be within the range of SSM/I*–TRMM*–AMSR-E retrieval. However, the long-term trends for the period with and without the SMMR* products show similar patterns, in agreement with changes in the concurrent rainfall and PET. These uncertainties should be kept in mind while using the merged products.

[44] Despite of these inherent uncertainties, this study confirmed the strong impact of ENSO on the near-surface hydrology across Australia and allowed some long-term trends in annual θ and τ to be identified and attributed. The agreements with previous studies and the model-derived

θ give us reasonable confidence in the time series of soil and vegetation moisture derived by the scaling method developed here. Development of a global data set along these lines should enable better estimation of hydrological variables and increase understanding of the impacts of ocean circulations on terrestrial hydrology and vegetation dynamics.

References

Anagnostou, E. N., A. J. Negri, and R. F. Adler (1999), Statistical adjustment of satellite microwave monthly rainfall estimates over Amazonia, *J. Appl. Meteorol.*, *38*, 1590–1598, doi:10.1175/1520-0450(1999)038<1590:SAOSMM>2.0.CO;2.

Armstrong, R. L., K. W. Knowles, M. J. Brodzik, and M. A. Hardman (1994), *DMSP SSM/I Pathfinder daily EASE-Grid brightness temperatures (July 1987 to December 2006)*, Natl. Snow and Ice Data Cent., Boulder, Colo. (Updated yearly.)

Atlas, D., D. Rosenfeld, and D. B. Wolff (1990), Climatologically tuned reflectivity-rain rate relations and links to area-time integrals, *J. Appl. Meteorol.*, *29*, 1120–1135, doi:10.1175/1520-0450(1990)029<1120:CTRRRR>2.0.CO;2.

Cashion, J., V. Lakshmi, D. Bosch, and T. J. Jackson (2005), Microwave remote sensing of soil moisture: Evaluation of the TRMM microwave imager (TMI) satellite for the Little River Watershed Tifton, Georgia, *J. Hydrol.*, *307*, 242–253, doi:10.1016/j.jhydrol.2004.10.019.

Cherkauer, K. A., L. C. Bowling, and D. P. Lettenmaier (2003), Variable infiltration capacity cold land process model updates, *Global Planet. Change*, *38*(1–2), 151–159, doi:10.1016/S0921-8181(03)00025-0.

Dai, A., I. Y. Fung, and A. D. Del Genio (1997), Surface observed global land precipitation variations during 1900–88, *J. Clim.*, *10*, 2943–2962, doi:10.1175/1520-0442(1997)010<2943:SOGLPV>2.0.CO;2.

De Jeu, R. A. M. (2003), Retrieval of land surface parameters using passive microwave observations, Ph.D. dissertation, 120 pp., Vrije Univ., Amsterdam.

De Jeu, R. A. M., and M. Owe (2003), Further validation of a new methodology for surface moisture and vegetation optical depth retrieval, *Int. J. Remote Sens.*, *24*, 4559–4578, doi:10.1080/0143116031000095934.

Derksen, C., E. LeDrew, A. Walker, and B. Goodison (2000), Influence of sensor overpass time on passive microwave-derived snow cover parameters, *Remote Sens. Environ.*, *71*, 297–308, doi:10.1016/S0034-4257(99)00084-X.

Dickinson, R. E., A. Henderson-Sellers, P. J. Kennedy, and M. F. Wilson (1986), Biosphere-atmosphere transfer scheme (BATS) for the NCAR Community Climate Model, *Tech. Note NCAR/TN-275+STR*, Natl. Cent. for Atmos. Res., Boulder, Colo.

Jackson, T. J., and P. E. O'Neill (1990), Attenuation of soil microwave emission by corn and soybeans at 1.4 and 5 GHz, *IEEE Trans. Geosci. Remote Sens.*, 28, 978–980, doi:10.1109/36.58989.

Jackson, T. J., and T. J. Schmugge (1991), Vegetation effects on the microwave emission from soils, *Remote Sens. Environ.*, 36, 203–212, doi:10.1016/0034-4257(91)90057-D.

Jackson, T. J., and T. J. Schmugge (1995), Surface soil moisture measurement with microwave radiometry, *Acta Astronaut.*, 35, 477–482, doi:10.1016/0094-5765(94)00288-W.

Kirdiashev, K. P., A. A. Chukhlantsev, and A. M. Shutko (1979), Microwave radiation of the Earth's surface in the presence of vegetation cover, *Radiotekh. Elektron.*, 24(2), 256–264.

Liang, X., D. P. Lettenmaier, E. F. Wood, and S. J. Burges (1994), A simple hydrologically based model of land surface water and energy fluxes for general circulation models, *J. Geophys. Res.*, 99(D7), 14,415–14,428, doi:10.1029/94JD00483.

Liu, Y., R. A. M. de Jeu, A. I. J. M. van Dijk, and M. Owe (2007), TRMM-TMI satellite observed soil moisture and vegetation density (1998–2005) show strong connection with El Niño in eastern Australia, *Geophys. Res. Lett.*, 34, L15401, doi:10.1029/2007GL030311.

McBride, J. L., and N. Nicholls (1983), Seasonal relationships between Australian rainfall and the southern oscillation, *Mon. Weather Rev.*, 111, 1998–2004, doi:10.1175/1520-0493(1983)111<1998:SRBARA> 2.0.CO;2.

McPhaden, M. J., S. E. Zebiak, and M. H. Glantz (2006), ENSO as an integrating concept in Earth science, *Science*, 314, 1740–1745, doi:10.1126/science.1132588.

Meesters, A. G. C. A., R. A. M. de Jeu, and M. Owe (2005), Analytical derivation of the vegetation optical depth from the microwave polarization difference index, *IEEE Trans. Geosci. Remote Sens.*, 2, 121–123, doi:10.1109/LGRS.2005.843983.

Njoku, E. G., and D. Entekhabi (1996), Passive microwave remote sensing of soil moisture, *J. Hydrol.*, 184, 101–129, doi:10.1016/0022-1694(95)02970-2.

Ogallo, L. J. (1988), Relationship between seasonal rainfall in East Africa and the Southern Oscillation Index, *J. Climatol.*, 8, 31–43, doi:10.1002/joc.3370080104.

Owe, M., R. A. M. de Jeu, and J. P. Walker (2001), A methodology for surface soil moisture and vegetation optical depth retrieval using the microwave polarization difference index, *IEEE Trans. Geosci. Remote Sens.*, 39, 1643–1654, doi:10.1109/36.942542.

Owe, M., R. A. M. de Jeu, and T. Holmes (2008), Multisensor historical climatology of satellite-derived global land surface moisture, *J. Geophys. Res.*, 113, F01002, doi:10.1029/2007JF000769.

Pauwels, V. R. N., R. Hoeben, N. E. C. Verhoest, and F. P. De Troch (2001), The importance of the spatial patterns of remotely sensed soil moisture in the improvement of discharge predictions for small-scale basins through data assimilation, *J. Hydrol.*, 251(1–2), 88–102, doi:10.1016/S0022-1694(01)00440-1.

Raju, S., A. Chanzy, J. Wigneron, J. Calvet, Y. Kerr, and L. Laguerre (1995), Soil moisture and temperature profile effects on microwave emission at low frequencies, *Remote Sens. Environ.*, 54, 85–97, doi:10.1016/0034-4257(95)00133-L.

Reichle, R. H., and R. D. Koster (2004), Bias reduction in short records of satellite soil moisture, *Geophys. Res. Lett.*, 31, L19501, doi:10.1029/2004GL020938.

Reichle, R. H., R. D. Koster, P. Liu, S. P. P. Mahanama, E. G. Njoku, and M. Owe (2007), Comparison and assimilation of global soil moisture retrievals from the Advanced Microwave Scanning Radiometer for the Earth Observing System (AMSR-E) and the Scanning Multichannel Microwave Radiometer (SMMR), *J. Geophys. Res.*, 112, D09108, doi:10.1029/2006JD008033.

Rodell, M., et al. (2004), The Global Land Data Assimilation System, *Bull. Am. Meteorol. Soc.*, 85(3), 381–394, doi:10.1175/BAMS-85-3-381.

Ropelewski, C. F., and M. S. Halpert (1987), Global and regional precipitation patterns associated with the El-Niño/Southern Oscillation, *Mon. Weather Rev.*, 115, 1606–1626, doi:10.1175/1520-0493(1987) 115<1606:GARSPP>2.0.CO;2.

Wagner, W., V. Naeimi, K. Scipal, R. A. M. de Jeu, and J. M. Fernandez (2007), Soil moisture from operational meteorological satellites, *Hydrogeol. J.*, 15, 121–131, doi:10.1007/s10040-006-0104-6.

Walker, J. P., and P. R. Houser (2001), A methodology for initializing soil moisture in a global climate model: Assimilation of near-surface soil moisture observations, *J. Geophys. Res.*, 106(D11), 11,761–11,774, doi:10.1029/2001JD900149.

Wentz, F. J., and M. C. Schabel (2000), Precise climate monitoring using complementary satellite data sets, *Nature*, 403, 414–416, doi:10.1038/35000184.

Wigmosta, M. S., L. W. Vail, and D. P. Lettenmaier (1994), A distributed hydrology-vegetation model for complex terrain, *Water Resour. Res.*, 30(6), 1665–1679, doi:10.1029/94WR00436.

Wigneron, J. P., P. Ferrazzoli, J. C. Calvet, Y. H. Kerr, and P. Bertuzzi (1999), A parametric study on passive and active microwave observations over a soybean crop, *IEEE Trans. Geosci. Remote Sens.*, 37(6), 2728–2733, doi:10.1109/36.803421.

Wood, E. F. (1991), Global scale hydrology: Advances in land surface modeling, *U.S. Natl. Rep. Int. Union Geod. Geophys. 1987–1990*, *Rev. Geophys.*, 29, 193–201.

———————————

R. A. M. de Jeu and T. R. H. Holmes, Department of Hydrology and Geo-Environmental Sciences, Faculty of Earth and Life Sciences, Vrije Universiteit, De Boelelaan 1085, NL-1081 HV Amsterdam, Netherlands.

Y. Y. Liu, School of Civil and Environmental Engineering, University of New South Wales, Sydney, NSW 2052, Australia. (yiliu001@gmail.com)

A. I. J. M. van Dijk, Black Mountain Laboratory, CSIRO Land and Water, GPO 1666, Canberra, ACT 2601, Australia.